

Remote control of myosin and kinesin motors using light-activated gearshifting

Muneaki Nakamura^{1,2}, Lu Chen², Stuart C. Howes³, Tony D. Schindler², Eva Nogales^{4,5,6} and Zev Bryant^{2,7}*

Cytoskeletal motors perform critical force generation and transport functions in eukaryotic cells^{1,2}. Engineered modifications of motor function provide direct tests of protein structure-function relationships and potential tools for controlling cellular processes or for harnessing molecular transport in artificial systems^{3,4}. Here, we report the design and characterization of a panel of cytoskeletal motors that reversibly change gears—speed up, slow down or switch directions—when exposed to blue light. Our genetically encoded structural designs incorporate a photoactive protein domain to enable light-dependent conformational changes in an engineered lever arm. Using *in vitro* motility assays, we demonstrate robust spatiotemporal control over motor function and characterize the kinetics of the optical gearshifting mechanism. We have used a modular approach to create optical gearshifting motors for both actin-based and microtubule-based transport.

Previously, the activity of cytoskeletal motors has been controlled *in vitro* by relying on inherent responses to environmental signals such as heat⁵ and by using natural or engineered^{6,7} responses to metal ions. Optical control has been explored using synthetic approaches such as covalent attachment of caging groups^{8,9} or photoswitches¹⁰, photolysis of tethers in multimotor teams¹¹ and modification of the adenosine triphosphate (ATP) fuel¹². To enable simple and precise control over nanoscale motion, we sought to create autonomous genetically encoded motors that can be specifically and reversibly switched between functional states using a spatially restricted signal.

Several properties of myosin motors can, in principle, be controlled by modulating the geometry and mechanics of the lever arm, which serves as a structural amplifier of conformational changes in the catalytic head. Protein engineering studies have confirmed that the size and direction of the force-generating power stroke depend on the length and exit angle of the lever arm^{13–15}. We previously designed a conformational change in an engineered lever arm to enable dynamic control over myosin directionality^{7,16}. We attached a collapsible lever arm element to an engineered variant of the (–)-end-directed myosin VI motor, and showed that the construct could be switched between (–)- and (+)-end-directed motion using a rigid-to-flexible transition triggered by [Ca²⁺]. We have speculated⁷ that a variation of this general approach could allow optical control of directionality and other motor properties.

The light–oxygen–voltage-sensing LOV2 protein domain, found in plant phototropins, responds to blue light with a structural transition¹⁷ that involves undocking of a C-terminal α -helix (Fig. 1a). The LOV2 domain from *Avena sativa* has been used in a variety

of chimaeric fusions to generate novel optical control of protein function^{18–21}. We hypothesized that conformational changes in the LOV2 domain could provide a basis for optical control of lever arm structure.

Guided by a structural model of the myosin VI power stroke²², we fused the catalytic domain of myosin VI to an artificial compound lever arm composed of the LOV2 domain flanked by rigid structural elements derived from α -actinin (Fig. 1b). α -Actinin fragments containing one (1R) or two (2R) spectrin-like repeats have been used extensively as functional replacements for myosin lever arms^{7,14,15,23,24}. We selected a myosin: α -actinin junction used in previous protein engineering studies of myosin VI directionality determinants^{7,15}, and additional helix-sharing junctions were designed between the α -actinin elements and the N- and C-termini of the LOV2 domain.

In the dark state, the tip of the compound lever arm is predicted to move toward the (+)-end of the actin filament (Fig. 1c, Supplementary Movie 1), leading to (+)-end-directed motility. When exposed to blue light, the C-terminal $\text{J}\alpha$ -helix of the LOV2 domain is expected to undock, changing the structural role of the LOV2 domain from a rigid hairpin to a flexible hinge (Fig. 1c). Because the C-terminal portion of the lever arm no longer contributes mechanically, the effective lever arm ends at the LOV2 domain, which moves toward the (–)-end of the actin filament during the power stroke (Fig. 1c, Supplementary Movie 1). This construct is therefore predicted to be a (–)-end-directed motor in blue light. In this scheme, the LOV2 domain serves to conditionally redirect the lever arm, analogous to the permanent redirection of a myosin lever arm using a four-helix bundle in a previous study¹⁴.

We created a series of monomeric myosin-1R-LOV2-2R (MyLOV) fusion constructs and tested their behaviour in gliding filament assays. Our initial design (MyLOV0) showed constitutive (–)-end-directed motion, and we did not detect significant light-dependent changes in velocity (Supplementary Table 1). We hypothesized that this failure might be due to undesired flexibility at helix-sharing domain junctions. In a previous study of engineered myosin VI motors, the myosin: α -actinin fusion point was varied to find optimal chimaeras, and successful fusion points were predicted with the help of molecular dynamics simulations¹⁵. Here, we have created junctional variants (Fig. 1b, Supplementary Fig. 1a) by including additional LOV2 residues at the N- and C-termini of the photoreceptor domain (MyLOV1 and MyLOV2) or by introducing computationally predicted mutations (see Supplementary Methods) in α -actinin residues near the LOV2 junctions (MyLOV3). After light-modulated myosin function was observed

¹Department of Chemistry, Stanford University, Stanford, California 94305, USA, ²Department of Bioengineering, Stanford University, Stanford, California 94305, USA, ³Biophysics Graduate Group, University of California, Berkeley, California 94720, USA, ⁴Department of Molecular and Cell Biology, University of California, Berkeley, California 94720, USA, ⁵Howard Hughes Medical Institute, University of California, Berkeley, California 94720, USA, ⁶Life Sciences Division, Lawrence Berkeley National Laboratory, Berkeley, California 94720, USA, ⁷Department of Structural Biology, Stanford University School of Medicine, Stanford, California 94305, USA. *e-mail: zevry@stanford.edu

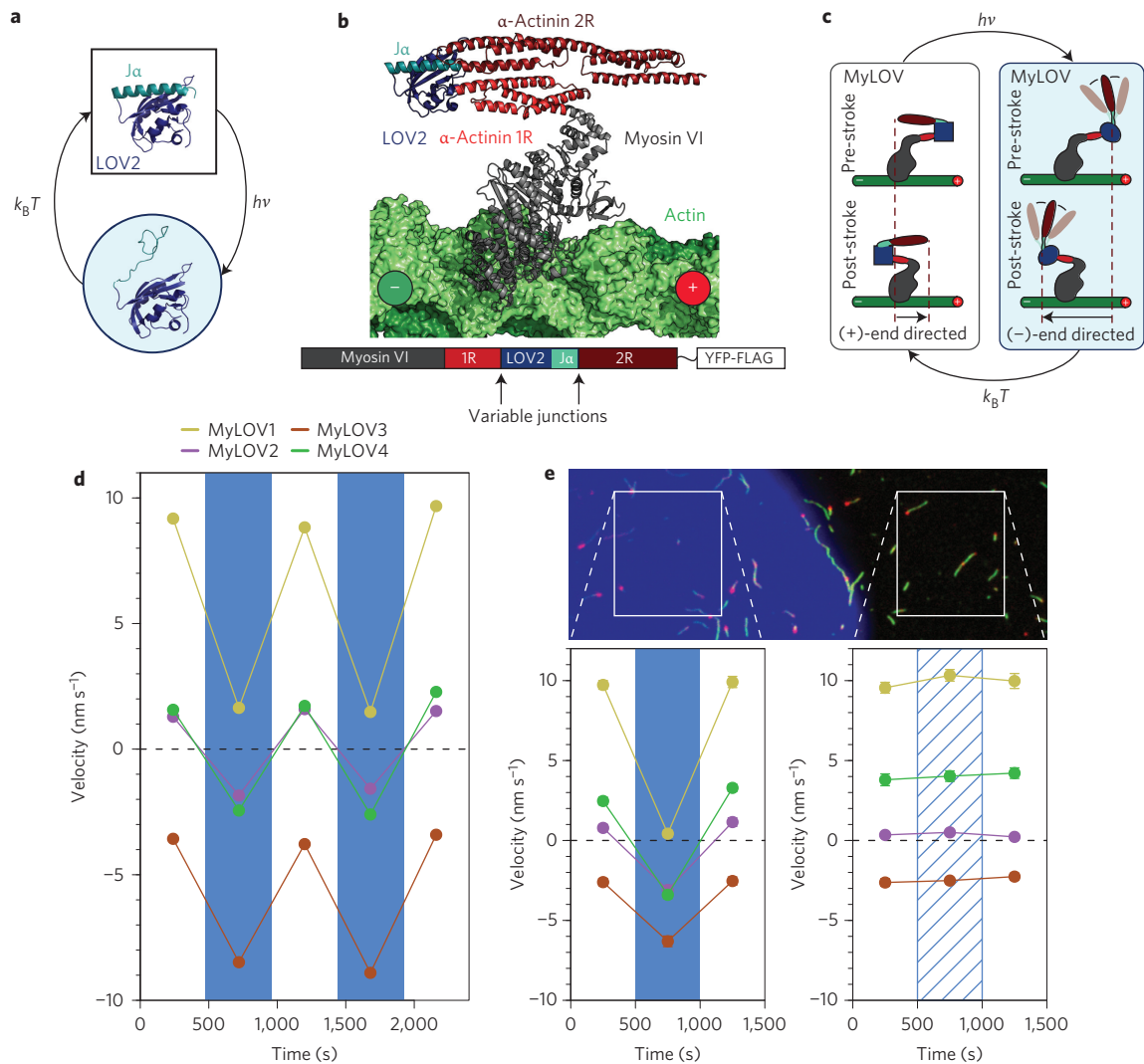


Figure 1 | Molecular design, proposed switching mechanism and *in vitro* performance of MyLOV constructs. **a**, The LOV2 domain undergoes a reversible conformational change in response to light¹⁷. **b**, Annotated ribbon diagram of the MyLOV design shown in the post-stroke state, with labels indicating structural modules and the modelled actin filament. A block diagram (below) indicates which junction regions were varied (Supplementary Fig. 1) in different MyLOV constructs. **c**, Cartoon of the MyLOV switching mechanism. In the dark (left), the compound lever arm is rigid and the tip of the lever arm moves toward the (+)-end of the actin filament during the power stroke (Supplementary Movie 1). When exposed to blue light (right), the α -helix undocks from the LOV2 domain and the C-terminal portion of the lever arm no longer contributes to the mechanical stroke, resulting in (-)-end-directed motion. **d,e**, Gliding filament results for MyLOV motors under intermittent blue illumination: full-field illumination (**d**; see Supplementary Movies 2–4) and restricted illumination (**e**; see Supplementary Movies 5–7). In **d**, filament velocity (mean \pm s.e.m.) is plotted for successive periods in which blue LED illumination was withheld (white background) or applied (blue background). Each point represents 17–138 filaments averaged over experiments repeated for two to four separate preparations of motor. Standard errors are smaller than the symbols for these data. In **e**, a field stop was used to partially mask the LED illumination (top). Filament velocities are shown for filaments within the restricted illumination area (left) and for filaments in the masked region (right). Masked filaments do not show any change in velocity during the illumination time (blue hatched background). Each point represents 9–34 filaments averaged over two to three motor preparations.

in the second-generation constructs, a third-generation chimaera (MyLOV4) was constructed by recombining the MyLOV1 and MyLOV3 sequences.

These four redesigned chimaeras (MyLOV1–MyLOV4) all show reversible changes in velocity under blue light illumination during *in vitro* motility (Fig. 1d, Supplementary Movies 2–4, Supplementary Table 1). MyLOV2 and MyLOV4 are (+)-end-directed in the dark and switch to (-)-end-directed motility when illuminated, as predicted from our original MyLOV design. MyLOV1 and MyLOV3 exhibit related behaviours that may be attributable to variations in junction angles or flexibility: MyLOV1 switches from faster (+)-end-directed motility to slower (+)-end-directed motility, and MyLOV3 switches from slower

(-)-end-directed motility to faster (-)-end-directed motility. In each of these cases, the change in velocity occurs in the expected direction, with the velocity becoming more (-)-end-directed upon illumination. Directionality switching is thus seen to be a special case of velocity switching.

An important feature of optical signals is that they may be readily controlled in both space and time^{25,26}. To demonstrate spatiotemporal control over myosin function, we tested MyLOV constructs using gliding filament assays in which blue illumination was intermittently applied to a restricted region of the field of view (Fig. 1e, Supplementary Movies 5–7). As expected, filaments in the restricted region showed characteristic light-dependent changes in velocity, whereas filaments in the adjacent masked region were unaffected.

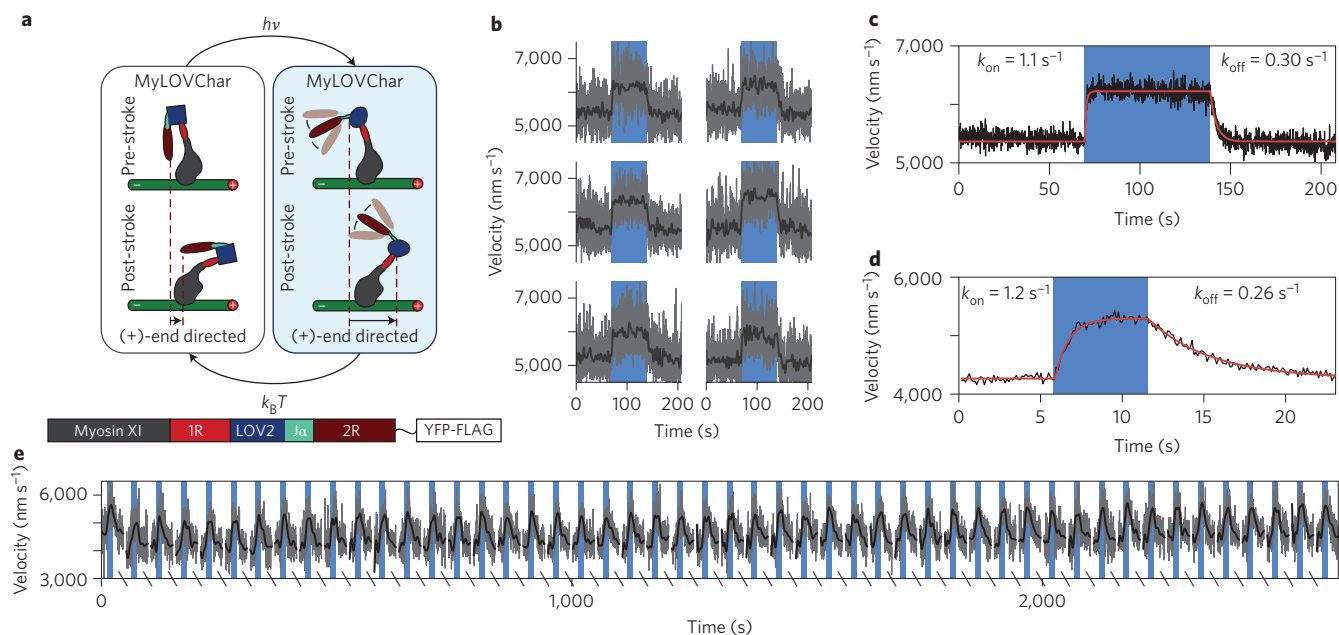


Figure 2 | Dynamic control of speed in MyLOVChar. **a**, Cartoon of the expected switching behaviour of MyLOVChar, showing that light-triggered undocking of the α -helix should increase the speed of (+)-end-directed motility. **b**, Sample traces of velocity versus time for individual high-speed gliding filament assays. Each plot shows the evolution of average filament velocity measured frame to frame at 8.65 Hz (grey) and low-pass-filtered to 1 Hz (black). Blue backgrounds indicate periods of LED illumination, and white backgrounds indicate periods in which illumination was withheld. **c**, Aligned average of 17 movies acquired using the protocol in **b**. Each data point (black) represents the averaged frame-to-frame speed of >500 filaments. Labelled rate constants were obtained from exponential fits (red) to the rise and decay in velocity, with best-fit dark velocity $v_1 = 5,370 \pm 40 \text{ nm s}^{-1}$ and light velocity $v_2 = 6,220 \pm 70 \text{ nm s}^{-1}$. **d**, **e**, A single field of view was illuminated with 50 pulses of blue light. Data acquisition was paused for 30 s between each acquisition/pulse cycle. In **d**, the aligned average velocity of all repeats, each point reflects the average frame-to-frame speed of >1,000 filaments is shown together with labelled exponential fits to the rise and fall in velocity (red). In **e**, a time trace of the entire 50-repeat experiment is shown. Frame-to-frame average filament velocities (grey) are shown together with low-pass-filtered data (black). Breaks in the axis indicate 30 s gaps between acquisitions.

Our results may be more generally applicable if the photoactive compound lever arm (1R-LOV2-2R) retains its function when ported to new molecular motor contexts. As an initial test of modularity, we created MyLOVChar monomers by grafting the photoactive lever arm from MyLOV4 onto the motor domain of *Chara corallina* myosin XI (Fig. 2a). For this construct we adopted a myosin: α -actinin fusion point that has been used previously for studies of recombinant *Chara* myosin^{16,24}. Myosin XI differs structurally and functionally from myosin VI: it is (+)-end-directed²⁷ and drives motility at much higher velocities²⁴. Based on the new structural context, illumination of MyLOVChar was predicted to cause a switch from slower to faster (+)-end-directed motility (Fig. 2a). As expected, MyLOVChar shows an increase in velocity that coincides sharply with illumination timing (Fig. 2b, Supplementary Movie 8).

Velocity measurements for MyLOV1–4 constructs relied on long integration times because of the low gliding filament speeds (substantially slower than reported for myosin VI constructs that retain the native calmodulin-binding domains; for example, 80 nm s^{-1} in ref. 28). In contrast, MyLOVChar exhibits rapid motility (albeit slower than the $30\text{--}60 \mu\text{m s}^{-1}$ speeds reported for native *Chara* myosin²⁹), facilitating measurements of velocity changes at high time resolution. We therefore used MyLOVChar to characterize the photoswitching kinetics of the photoactive lever arm. Frame-to-frame filament velocities were analysed at subsecond resolution, revealing an exponential rise in velocity upon illumination and a subsequent decay in velocity when illumination was removed (Fig. 2c,d). Switching occurs on a timescale of seconds, with a shorter decay time than has been observed in some previous LOV2 fusions¹⁸ or for the isolated *Avena sativa* LOV2 domain^{30,31}. We further tested the repeatability of the photoswitch by subjecting MyLOVChar to successive short

pulses of light stimulation, and observed no sign of photofatigue over 50 repetitions (Fig. 2e).

We have shown that a design based on light-triggered conformational changes in an artificial lever arm can be applied to control the behaviour of distinct myosin classes. To further challenge the modularity of our approach, we asked whether light-activated gearshifting could be extended to control motors that act on microtubules. Unlike conventional kinesin-1, the non-claret disjunctional protein (Ncd) motor and other members of the kinesin-14 family have been proposed to use a swinging lever arm mechanism reminiscent of myosin, where the coiled-coil domain of the Ncd dimer is thought to act as an extended lever arm structure^{32–34}. As a step toward adapting our gearshifting design to Ncd, we first sought to create monomeric Ncd motors in which the coiled-coil is functionally replaced with an artificial lever arm. We created 1R-Ncd by fusing an α -actinin spectrin repeat to the catalytic head of Ncd (Fig. 3a), imitating previous engineered myosin designs. As expected (Fig. 3b), 1R-Ncd is a (–)-end-directed kinesin (Supplementary Movie 9), with gliding filament velocities faster than the catalytic domain alone and similar to an Ncd construct with a truncated native coiled-coil lever arm (Supplementary Table 2), although slower than the $>100 \text{ nm s}^{-1}$ velocities typical of intact Ncd motors³³. Further validation is provided by a cryoelectron microscopy reconstruction of 1R-Ncd, which shows the artificial lever arm in the expected orientation in the post-stroke state (Fig. 3c, Supplementary Movie 10).

We next created two optically controllable microtubule-based motors, LOVKinA and LOVKinB, by fusing the catalytic domain of Ncd to truncated variants of the compound lever arm from MyLOV4 (Fig. 3d,e). As expected, LOVKinA is (+)-end-directed in the dark and becomes (–)-end-directed upon illumination

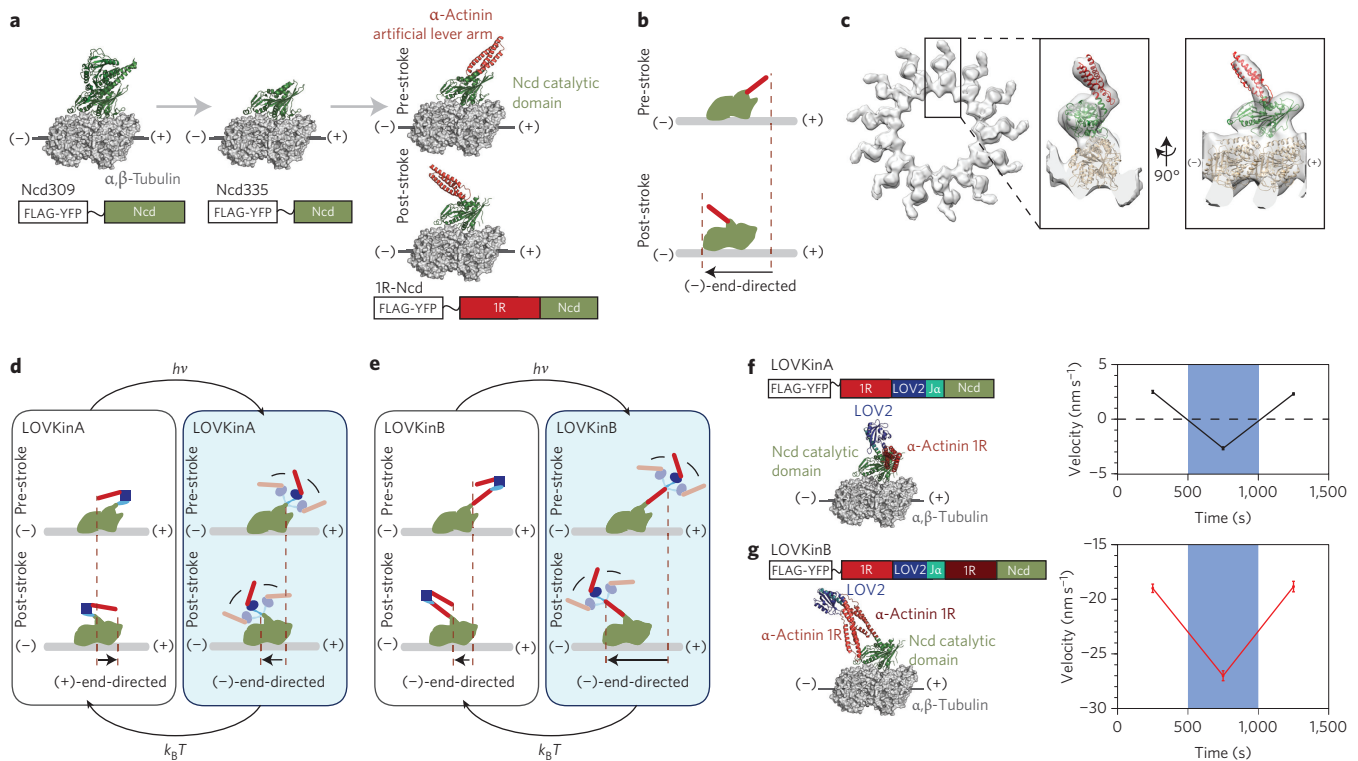


Figure 3 | Design, structure and *in vitro* performance of engineered kinesin-14 motors. **a**, Structural models illustrating truncation of Ncd and fusion of an artificial lever arm. Ribbon diagrams of the 1R-Ncd design are shown in both pre- and post-stroke states, based on the two conformations of Ncd seen in 3L1C (ref. 39). **b**, Cartoon depicting the (-)-end-directed power stroke of 1R-Ncd. **c**, Three-dimensional cryoelectron microscopy map of microtubules decorated with 1R-Ncd in 5 mM adenyllyl imidodiphosphate (AMP-PNP) with docked models of tubulin (1JFF) and 1R-Ncd in the expected post-stroke state. **d,e**, Cartoons explaining the switching behaviour of LOVKin constructs. **f,g**, Ribbon diagrams of LOVKin constructs are shown in the post-stroke state together with plots of filament velocities (mean \pm s.e.m.) acquired under intermittent full-field blue illumination. Each point represents 28–43 filaments averaged over one to three motor preparations. An additional preparation assayed with slightly longer acquisition times also showed similar results (Supplementary Table 3).

(Fig. 3f, Supplementary Movie 11). A point mutant of Ncd has previously been reported to be stochastically bidirectional³⁵. LOVKinA now places bidirectionality under the deterministic control of an external signal. As shown previously for myosin¹⁴, successful geometric redirection of the lever arm provides additional support for a swinging lever arm model for Ncd. LOVKinB is (-)-end-directed, and shows a velocity change in the expected direction, with increased speed in the light (Fig. 3g, Supplementary Movie 12).

We have shown that spatiotemporal control of both actin-based and microtubule-based motors can be achieved using a general design based on light-triggered conformational changes in an artificial lever arm. Switching behaviours are qualitatively predicted by structural models of the pre- and post-stroke states of the engineered motors, although further structural and single-molecule measurements may be required to develop accurate quantitative models of light-dependent behaviours (Supplementary Fig. 2, Supplementary Note). Desirable extensions of our molecular designs will include building from monomeric motors to switchable processive multimers, as previously demonstrated for $[Ca^{2+}]$ -controlled bidirectional myosins^{7,16}. In future applications of this work, genetically encoded light-responsive motors may expand the optogenetics toolkit, complementing precise perturbations of ion channels²⁶ and intracellular signalling²⁵ with spatiotemporal control of cytoskeletal transport and contractility. Light-activated gearshifting will enable new synthetic approaches in cell biology⁴, new investigations of basic properties of active fluids³⁶ and dynamic control of analyte transport in microfabricated devices that harness the proven capabilities of biological molecular motors^{3,4,37}.

Methods

Molecular constructs. Constructs were assembled from DNA fragments encoding porcine myosin VI codons 1–790, *Chara corallina* myosin XI codons 1–746, *Dictyostelium discoideum* α -actinin codons 266–502 (with construct-dependent truncations and mutations as indicated), *Avena sativa* phot1 codons 408–543 (extended for certain constructs, as indicated) and *Drosophila melanogaster* Ncd codons 309–700 (with further N-terminal truncations as indicated) and cloned into an expression plasmid based on pBiex-1 (Novagen) that includes the codons for a C-terminal eYFP and FLAG tag (DYKDDDDK). Proteins were expressed via transient transfection of SF9 cells and affinity purified as described previously⁷. For details of construct composition, including junction variations, see Supplementary Fig. 1.

Motility assays. MyLOV constructs were characterized using dual-labelled gliding filament assays as described previously⁷, using a modified assay buffer containing 23 mM Tris-HCl (pH 7.5), 23 mM KCl, 9.2 mM dithiothreitol (DTT), 1.9 mM $MgCl_2$, 0.94 mM EGTA, 0.75 mM imidazole-HCl, 2.0 mM ATP, 1.5% (vol/vol) glycerol, an ATP regeneration system containing 1.0 mM phosphocreatine and $0.95 \mu g ml^{-1}$ creatine phosphokinase and an oxygen-scavenging system containing 0.40% (wt/vol) glucose, $0.20 mg ml^{-1}$ glucose oxidase and $0.36 \mu g ml^{-1}$ catalase. Each flow chamber was constructed using a Nescofilm gasket sandwiched between two glass coverslips, after spin-coating the assay surface of the imaging-side coverslip with nitrocellulose. Assays were prepared by incubating with anti-green fluorescent protein (anti-GFP; Millipore) to mediate specific attachment of the YFP-tagged motor, then blocking the surface with $2 mg ml^{-1}$ BSA (Sigma), and finally incubating with 100 nM motor for 2 min. TMR/Cy5-labelled filaments were excited with a 532 nm optically pumped semiconductor laser (Coherent) using total internal reflection and imaged on an electron-multiplying charge-coupled device camera (Andor). Blue illumination was provided by epi-illumination using a light-emitting diode (LED) with emission centred at 470 nm (Thorlabs) using custom software to control the LED power and timing. The estimated irradiance at the sample was $16 \pm 3 mW cm^{-2}$. All assays were carried out at room temperature ($23 \pm 1 ^\circ C$).

Ncd constructs were characterized using polarity-labelled microtubule filaments generated as previously described³⁸. Briefly, bright microtubule seeds were first

prepared by mixing 0.30 mg ml⁻¹ rhodamine-tubulin (Cytoskeleton) and 3.5 mg ml⁻¹ unlabelled tubulin (Cytoskeleton) in BRB80 (80 mM K-PIPES, 1 mM MgCl₂, 1 mM EGTA, pH 6.8) with 10% dimethylsulphoxide and 1 mM guanosine triphosphate (GTP), then incubating at 37 °C for 10 min. A polymerization mixture for the more dimly labelled microtubule extension was prepared with 0.014 mg ml⁻¹ rhodamine-labelled tubulin, 0.6 mg ml⁻¹ unlabelled tubulin and 0.6 mg ml⁻¹ N-ethylmaleimide (NEM)-modified tubulin. Filaments were assembled by combining 1.5 µl of the bright seeds with 18 µl of the polymerization mixture and incubating at 37 °C for 15 min before adding 20 µM taxol. Gliding filament assays were performed in a buffer containing 80 mM K-PIPES (pH 6.8), 100 mM KCl, 2 mM MgCl₂, 1 mM EGTA, 10 mM DTT, 20 µM taxol and 1 mM ATP, supplemented with the ATP-regeneration and oxygen-scavenging systems used for MyLOV constructs. Assays were prepared and imaged as described for the MyLOV constructs above, except that the motor was incubated at a concentration of 1 µM and blocking was carried out using 1 mg ml⁻¹ BSA.

Videomicroscopy analysis. For MyLOV1–4 data, signed velocities were determined for each 8 min period of illumination or darkness using automated analysis of videomicroscopy data. In this analysis, filaments were only selected for analysis if they were associated with a single Cy5-labelled seed, enabling unambiguous directionality determination. A low-order polynomial was fit to each filament's trajectory over each eight-minute segment, and the contour length was used to determine the displacement over that period. For MyLOVChar data, filaments were automatically identified and tracked, and displacements for each filament were calculated frame-to-frame. For Ncd constructs, unambiguous polarity-labelled filaments were manually selected and analysed by measuring linear displacements of the leading filament end.

Received 31 March 2014; accepted 19 June 2014;
published online 3 August 2014

References

- Sellers, J. R. Myosins: a diverse superfamily. *Biochim. Biophys. Acta* **1496**, 3–22 (2000).
- Vale, R. D. The molecular motor toolbox for intracellular transport. *Cell* **112**, 467–480 (2003).
- Goel, A. & Vogel, V. Harnessing biological motors to engineer systems for nanoscale transport and assembly. *Nature Nanotech.* **3**, 465–475 (2008).
- Goodman, B. S., Derr, N. D. & Reck-Peterson, S. L. Engineered, harnessed, and hijacked: synthetic uses for cytoskeletal systems. *Trends Cell Biol.* **22**, 644–652 (2012).
- Korten, T., Birnbaum, W., Kuckling, D. & Diez, S. Selective control of gliding microtubule populations. *Nano Lett.* **12**, 348–353 (2012).
- Cochran, J. C., Zhao, Y. C., Wilcox, D. E. & Kull, F. J. A metal switch for controlling the activity of molecular motor proteins. *Nature Struct. Mol. Biol.* **19**, 122–127 (2012).
- Chen, L., Nakamura, M., Schindler, T. D., Parker, D. & Bryant, Z. Engineering controllable bidirectional molecular motors based on myosin. *Nature Nanotech.* **7**, 252–256 (2012).
- Marriott, G. & Heidecker, M. Light-directed generation of the actin-activated ATPase activity of caged heavy meromyosin. *Biochemistry* **35**, 3170–3174 (1996).
- Goguen, B. N., Hoffman, B. D., Sellers, J. R., Schwartz, M. A. & Imperiali, B. Light-triggered myosin activation for probing dynamic cellular processes. *Angew. Chem. Int. Ed.* **50**, 5667–5670 (2011).
- Yamada, M. D., Nakajima, Y., Maeda, H. & Maruta, S. Photocontrol of kinesin ATPase activity using an azobenzene derivative. *J. Biochem.* **142**, 691–698 (2007).
- Derr, N. D. *et al.* Tug-of-war in motor protein ensembles revealed with a programmable DNA origami scaffold. *Science* **338**, 662–665 (2012).
- Kamei, T., Fukaminato, T. & Tamaoki, N. A photochromic ATP analogue driving a motor protein with reversible light-controlled motility: controlling velocity and binding manner of a kinesin-microtubule system in an *in vitro* motility assay. *Chem. Commun.* **48**, 7625–7627 (2012).
- Uyeda, T. Q., Abramson, P. D. & Spudich, J. A. The neck region of the myosin motor domain acts as a lever arm to generate movement. *Proc. Natl Acad. Sci. USA* **93**, 4459–4464 (1996).
- Tsiavalariis, G., Fujita-Becker, S. & Manstein, D. J. Molecular engineering of a backwards-moving myosin motor. *Nature* **427**, 558–561 (2004).
- Liao, J.-C., Elting, M. W., Delp, S. L., Spudich, J. A. & Bryant, Z. Engineered myosin VI motors reveal minimal structural determinants of directionality and processivity. *J. Mol. Biol.* **392**, 862–867 (2009).
- Schindler, T. D., Chen, L., Lebel, P., Nakamura, M. & Bryant, Z. Engineering myosins for long-range transport on actin filaments. *Nature Nanotech.* **9**, 33–38 (2014).
- Harper, S. M., Neil, L. C. & Gardner, K. H. Structural basis of a phototropin light switch. *Science* **301**, 1541–1544 (2003).
- Lee, J. *et al.* Surface sites for engineering allosteric control in proteins. *Science* **322**, 438–442 (2008).
- Strickland, D., Moffat, K. & Sosnick, T. R. Light-activated DNA binding in a designed allosteric protein. *Proc. Natl Acad. Sci. USA* **105**, 10709–10714 (2008).
- Wu, Y. I. *et al.* A genetically encoded photoactivatable Rac controls the motility of living cells. *Nature* **461**, 104–108 (2009).
- Strickland, D. *et al.* TULIPs: tunable, light-controlled interacting protein tags for cell biology. *Nature Methods* **9**, 379–384 (2012).
- Ménétrey, J., Llinas, P., Mukherjee, M., Sweeney, H. L. & Houdusse, A. The structural basis for the large powerstroke of myosin VI. *Cell* **131**, 300–308 (2007).
- Anson, M., Geeves, M. A., Kurzawa, S. E. & Manstein, D. J. Myosin motors with artificial lever arms. *EMBO J.* **15**, 6069–6074 (1996).
- Ito, K. *et al.* Recombinant motor domain constructs of *Chara corallina* myosin display fast motility and high ATPase activity. *Biochem. Biophys. Res. Commun.* **312**, 958–964 (2003).
- Toettcher, J. E., Voigt, C. A., Weiner, O. D. & Lim, W. A. The promise of optogenetics in cell biology: interrogating molecular circuits in space and time. *Nature Methods* **8**, 35–38 (2011).
- Boyden, E. S., Zhang, F., Bamberg, E., Nagel, G. & Deisseroth, K. Millisecond-timescale, genetically targeted optical control of neural activity. *Nature Neurosci.* **8**, 1263–1268 (2005).
- Tominaga, M. *et al.* Higher plant myosin XI moves processively on actin with 35 nm steps at high velocity. *EMBO J.* **22**, 1263–1272 (2003).
- Bryant, Z., Altman, D. & Spudich, J. A. The power stroke of myosin VI and the basis of reverse directionality. *Proc. Natl Acad. Sci. USA* **104**, 772–777 (2007).
- Higashi-Fujime, S. *et al.* The fastest actin-based motor protein from the green algae, *Chara*, and its distinct mode of interaction with actin. *FEBS Lett.* **375**, 151–154 (1995).
- Salomon, M., Christie, J. M., Knieb, E., Lempert, U. & Briggs, W. R. Photochemical and mutational analysis of the FMN-binding domains of the plant blue light receptor, phototropin. *Biochemistry* **39**, 9401–9410 (2000).
- Alexandre, M. T. A., Arents, J. C., van Grondelle, R., Hellingwerf, K. J. & Kennis, J. T. M. A base-catalyzed mechanism for dark state recovery in the *Avena sativa* phototropin-1 LOV2 domain. *Biochemistry* **46**, 3129–3137 (2007).
- Yun, M. *et al.* Rotation of the stalk/neck and one head in a new crystal structure of the kinesin motor protein, Ncd. *EMBO J.* **22**, 5382–5389 (2003).
- Endres, N. F., Yoshioka, C., Milligan, R. A. & Vale, R. D. A lever-arm rotation drives motility of the minus-end-directed kinesin Ncd. *Nature* **439**, 875–878 (2006).
- Wendt, T. G. *et al.* Microscopic evidence for a minus-end-directed power stroke in the kinesin motor Ncd. *EMBO J.* **21**, 5969–5978 (2002).
- Endow, S. A. & Higuchi, H. A mutant of the motor protein kinesin that moves in both directions on microtubules. *Nature* **406**, 913–916 (2000).
- Schaller, V., Weber, C. A., Hammerich, B., Frey, E. & Bausch, A. R. Frozen steady states in active systems. *Proc. Natl Acad. Sci. USA* **108**, 19183–19188 (2011).
- Mansour, A. Translational actomyosin research: fundamental insights and applications hand in hand. *J. Muscle Res. Cell Motil.* **33**, 219–233 (2012).
- Hyman, A. A. Preparation of marked microtubules for the assay of the polarity of microtubule-based motors by fluorescence. *J. Cell Sci.* **14**(Suppl.), 125–127 (1991).
- Heuston, E., Bronner, C. E., Kull, F. J. & Endow, S. A. A kinesin motor in a force-producing conformation. *BMC Struct. Biol.* **10**, 19 (2010).

Acknowledgements

The authors thank J.-C. Liao, T. Omabegho, D.J. Cipriano, P.V. Ruijgrok and M.W. Elting for technical assistance, S. Sutton and H.M. Warrick for providing purified actin, and M.J. Footer for providing a gelsolin expression plasmid. This work was supported by a Pew Scholars Award, National Institutes of Health grants DP2 OD004690 (to Z.B.) and P01GM051487 (to E.N.), an AHA Predoctoral Fellowship (to M.N.), a National Science Foundation Graduate Research Fellowship (to L.C.) and a Stanford Graduate Fellowship (to T.D.S.). E.N. is a Howard Hughes Medical Institute investigator.

Author contributions

M.N. designed myosin constructs and performed myosin experiments. T.D.S. assisted with myosin research. L.C. and M.N. designed and assayed Ncd constructs, analysed all motility data and provided samples and assistance for electron microscopy. S.C.H. performed cryoelectron microscopy and obtained three-dimensional reconstructions. E.N. supervised cryoelectron microscopy research. Z.B. conceived and supervised the overall project. M.N., Z.B., L.C. and S.C.H. contributed to writing the paper. All authors discussed the results and commented on the manuscript.

Additional information

Supplementary information is available in the online version of the paper. Reprints and permissions information is available online at www.nature.com/reprints. Correspondence and requests for materials should be addressed to Z.B.

Competing financial interests

The authors declare no competing financial interests.